Journal of Alloys and Compounds 855 (2021) 157475

Contents lists available at ScienceDirect

Journal of Alloys and Compounds

journal homepage: http://www.elsevier.com/locate/jalcom

Catalytic effect of $SrTiO_3$ on the dehydrogenation properties of $LiAlH_4$

M. Ismail [a,*], N.A. Sazelee [a], N.A. Ali [a], S. Suwarno [b]

[a] Energy Storage Research Group, Faculty of Ocean Engineering Technology and Informatics, Universiti Malaysia Terengganu, 21030, Kuala Nerus, Malaysia
[b] Department of Mechanical Engineering, Institut Teknologi Sepuluh Nopember, Surabaya, 60111, Indonesia

ARTICLE INFO

Article history:
Received 6 September 2020
Received in revised form
2 October 2020
Accepted 5 October 2020
Available online 7 October 2020

Keywords:
Lithium alanates
Dehydrogenation properties
Strontium titanate
Catalytic effect

ABSTRACT

Lithium alanate ($LiAlH_4$) is regarded as one of the potential materials for on-board hydrogen storage applications because of its high hydrogen capacity. However, this advantage is restricted by several obstacles such as high decomposition temperature and slow desorption kinetics that deny its marketability. Hence, efforts such as decreasing the particle size by the mechanical milling technique and by adding dopants/catalysts have been investigated widely to overcome these drawbacks. In this work, the influences of strontium titanate ($SrTiO_3$) on the dehydrogenation properties of $LiAlH_4$ have been investigated for the first time. The onset decomposition temperature of the 10 wt% $SrTiO_3$-doped $LiAlH_4$ sample decreased from 145 °C to 80 °C in the first dehydrogenation step and from 178 °C to 120 °C in the second dehydrogenation step. For the desorption kinetic measurements at 90 °C, the 10 wt% $SrTiO_3$-doped $LiAlH_4$ sample could desorb about 3.0 wt% of H_2 in 20 min compared to 0.2 wt% by the as-milled $LiAlH_4$. The activation energies calculated by Kissinger analysis in the two-step dehydrogenation process of $LiAlH_4$ were lowered after the addition of $SrTiO_3$. From the X-ray diffraction analysis, we found that $SrTiO_3$ did not react during the mechanical milling and heating (desorption) processes. $SrTiO_3$ is believed to play a catalytic role by reducing the physical size of $LiAlH_4$ during the mechanical milling process thereby improving the dehydrogenation storage properties of $LiAlH_4$.

1. Introduction

Currently, metal hydrides and complex hydrides attracts a great attention as a solid-state hydrogen storage medium [1,2]. Metal hydrides (especially MgH_2) shows an outstanding reversible desorb/absorb hydrogen meanwhile complex hydrides such as $LiAlH_4$ and $NaBH_4$ has a high hydrogen storage capacity [3–7]. Theoretically, $LiAlH_4$ and $NaBH_4$ can desorb 7.9 wt% and 10.6 wt% of H_2, respectively. This hydrogen amount fulfils the U.S. Department of Energy 2020 goals for on-board vehicle applications (4.5 wt% of hydrogen) [8]. Although $LiAlH_4$ and $NaBH_4$ shows a promising characteristic as a solid-state hydrogen storage medium, its high desorption temperature and sluggish dehydrogenation kinetics hinder its wider applications.

To lower the decomposition temperature and improve the desorption kinetics of complex hydrides, several strategies have been carried out previously such as decreasing the particle sizes by mechanical milling [9,10], producing reactive hydride composites (mixed with other hydride materials) [11–13], doping with catalysts/additives [14–16] and regeneration process by hydrolysis [17–21]. From the literature, doping with catalysts/additives is the most active approach for the modification of $LiAlH_4$ as a potential material for hydrogen storage [3,22]. Catalysts/additives such as metals [23–25], metal oxides [26–28], metal halides [29,30], carbon-based materials [31,32] and hard materials [33,34] have been used as doping agents in enhancing the dehydrogenation characteristics of $LiAlH_4$.

Hard and brittle additives, such as TiC and SiC, have been reported to act as surface catalysts for metal/complex hydrides [33,35,36]. The results showed that the catalysts did not react with the host material during the mechanical milling process and during the de/rehydrogenation process. Rafi-ud-din et al. [33] claimed that the desorption properties of $LiAlH_4$ had improved after milling with nano-TiC. The addition of hard and brittle nano-TiC reduces the particle sizes and creates larger surface areas for hydrogen to interact, thus improving the dehydrogenation characteristics of $LiAlH_4$. Furthermore, Ranjbar et al. [36] stated that using a hard material, SiC, the grain size of the MgH_2 could decrease and reduce the agglomeration of MgH_2 crystallites; thus, further enhancing the ab/desorption kinetic properties of the MgH_2–SiC composite.

* Corresponding author.
E-mail address: mohammadismail@umt.edu.my (M. Ismail).

https://doi.org/10.1016/j.jallcom.2020.157475
0925-8388/

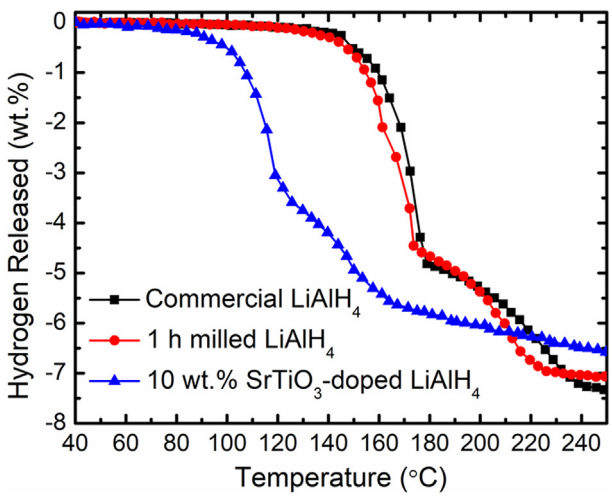

Fig. 1. Thermal decomposition temperature of commercial $LiAlH_4$, 1 h milled $LiAlH_4$, and $LiAlH_4$-10 wt% $SrTiO_3$ sample.

Therefore, motivated by the above-mentioned strategies, it is desirable to study the effects of other hard materials on the dehydrogenation properties of $LiAlH_4$.

Our previous studies have shown that $SrTiO_3$ is a promising catalyst for MgH_2 [37–39]. The results showed that the main catalytic role of the $SrTiO_3$ catalyst on MgH_2 is because of the hardness of $SrTiO_3$. From the X-ray diffraction (XRD) results, the $SrTiO_3$ phase was still unchanged after the mechanical milling and ab/desorption process, confirming that no reaction had occurred between MgH_2 and $SrTiO_3$. $SrTiO_3$ is believed to play a catalytic role by reducing the physical size of MgH_2 during the mechanical milling process. Inspired by these studies, in this study, $SrTiO_3$ was used as a catalyst to examine its influence on the hydrogen storage properties of $LiAlH_4$. It is reasonable to believe that $SrTiO_3$ could be an effective catalyst to lower the decomposition temperature and boost the dehydrogenation kinetics of $LiAlH_4$. According to the author's knowledge, this study is the first comprehensive work to examine the effect of the $SrTiO_3$ catalyst on the dehydrogenation behaviour of $LiAlH_4$.

2. Experimental details

All the chemicals in this work were used directly without any purification. $LiAlH_4$ powder (95% purity; Sigma-Aldrich) was milled with 10 wt% of $SrTiO_3$ (98% purity; Sigma-Aldrich) at 400 rpm for 1 h; the ratio of the steel balls to powder was about 30:1. The undoped $LiAlH_4$ was also milled mechanically using the same method for comparison purposes. All the preparation processes, such as weighing, were carried out in an atmosphere Ar-filled glovebox (Mbraun Unilab) to minimise oxidation.

The onset decomposition temperature and dehydrogenation kinetic measurements were examined using a Sieverts-type apparatus (Advanced Materials Corporation). To measure the onset decomposition temperature, a 300-mg sample was placed into the sample holder and heated from room temperature to 300 °C under vacuum at a heating rate of 5 °C/min. The dehydrogenation kinetic measurements were done at 90 °C under a hydrogen pressure of 0.1 MPa.

Differential scanning calorimetry (DSC) to investigate the thermal properties was carried out using the Mettler Toledo DSC/TGA under an Ar-flow atmosphere (30 mL/min). About 7 mg each of undoped and doped samples were placed into alumina crucibles and heated at various rates (15, 20, 25 and 30 °C/min) from room temperature to 300 °C.

Table 1
Comparison of onset decomposition temperature of $LiAlH_4$ doped with different catalysts.

System	Onset decomposition temperature (°C)	
	First stage	Second stage
$LiAlH_4$ + micro TiH_2 [40]	90.0	150.0
$LiAlH_4$ + TiN [41]	90.0	140.0
$LiAlH_4$ + NbN [42]	95.0	169.1
$LiAlH_4$ + nano Nb_2O_5 [43]	95.0	130.0
$LiAlH_4$ + $SrTiO_3$ [this work]	80.0	120.0

The phase confirmation of the samples was analysed by XRD (Rigaku MiniFlex X-ray diffractometer) with Cu–Kα radiation. The Fourier-transform infrared (FTIR) spectra of the samples were recorded using an infrared (IR) Tracer-100 Shimadzu within the wave number ranging from 800 to 2000 cm^{-1} with a spectral resolution of 4 cm^{-1}. The morphology of the undoped and doped samples was viewed by scanning electron microscopy (SEM; JEOL JSM–6350LA).

3. Result and discussions

Fig. 1 shows the thermal decomposition temperatures of the commercial $LiAlH_4$, 1-h milled $LiAlH_4$ and $LiAlH_4$–10 wt% $SrTiO_3$ samples. The commercial $LiAlH_4$ sample started to desorb hydrogen at 148 °C in the first dehydrogenation step and at 180 °C in the second dehydrogenation step. After milling for 1 h, the onset decomposition temperature of $LiAlH_4$ reduced slightly to about 145 °C and 178 °C in the first and second dehydrogenation steps, respectively. After adding 10 wt% of $SrTiO_3$, the onset decomposition temperature of $LiAlH_4$ decreased dramatically to 80 °C and 120 °C in the first and second dehydrogenation steps, respectively. From the results, it is obvious that the onset decomposition temperature of $LiAlH_4$ decreased remarkably in both steps of dehydrogenation after the addition of 10 wt% $SrTiO_3$. For display the catalytic effect of $SrTiO_3$ on the onset decomposition of $LiAlH_4$, the comparison of $LiAlH_4$ doped with different catalysts is showed in Table 1.

The next investigation was to study the influences of $SrTiO_3$ on the dehydrogenation kinetics of $LiAlH_4$. The dehydrogenation kinetics of the commercial $LiAlH_4$, 1-h milled $LiAlH_4$ and $LiAlH_4$–10 wt% $SrTiO_3$ samples were examined at a fixed temperature of 90 °C as shown in Fig. 2. From the results, we can see that the dehydrogenation kinetics rate of $LiAlH_4$ was enhanced after the addition of 10 wt% $SrTiO_3$. The $LiAlH_4$–10 wt% $SrTiO_3$ sample desorbed approximately 3.0 wt% H_2 at 90 °C within 20 min whereas the commercial and 1-h milled $LiAlH_4$ samples desorbed below 0.5 wt% of hydrogen in the same time. The dehydrogenation kinetic measurements revealed that the 10 wt% $SrTiO_3$-doped $LiAlH_4$ sample displayed an average dehydrogenation kinetics rate seven times quicker than that of the undoped $LiAlH_4$ samples. The comparison of dehydrogenation kinetic of $LiAlH_4$ doped with different catalysts is listed in Table 2.

The impact of the catalyst on the thermal event of $LiAlH_4$ was further examined by DSC as shown in Fig. 3. As can be seen, the thermal properties of the 1-h milled $LiAlH_4$ sample showed four curves corresponding to two endothermic and two exothermic events. The first exothermic and endothermic event peaks at 137 °C and 166 °C refer to the reaction of surface hydroxyl impurities with $LiAlH_4$ and the melting of $LiAlH_4$, respectively. The second exothermic and endothermic event peaks at 190 °C and 243 °C correspond to the decomposition of $LiAlH_4$ (first step of

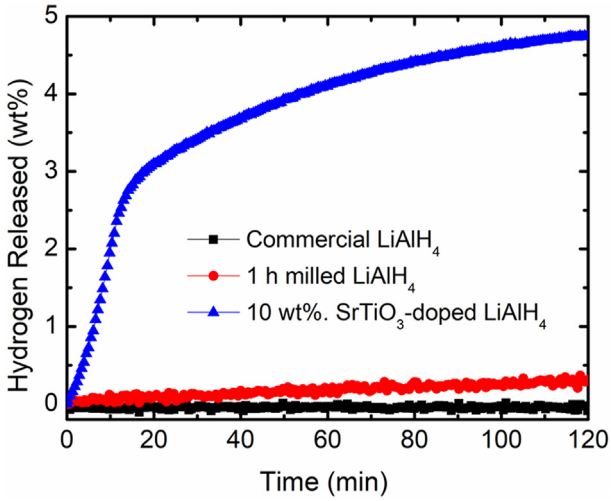

Fig. 2. Dehydrogenation kinetics of commercial $LiAlH_4$, 1 h milled $LiAlH_4$, and $LiAlH_4$-10 wt% $SrTiO_3$ sample.

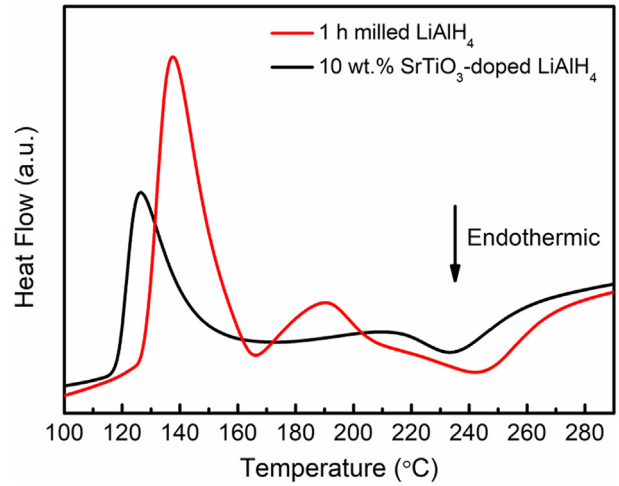

Fig. 3. Differential scanning calorimetry profiles of 1 h milled $LiAlH_4$ and $LiAlH_4$-10 wt % $SrTiO_3$ sample (heating rate 30 °C/min).

dehydrogenation; Eq. (1)) and the decomposition of Li_3AlH_6 (second step of dehydrogenation; Eq. 2). After 10 wt% of $SrTiO_3$ was added, the number of peaks reduced to two, of which one was exothermic and the other was endothermic, and this occurred at a lower temperature. The exothermic peak (decomposition of $LiAlH_4$) occurred at 126 °C, while the endothermic peaks (decomposition of Li_3AlH_6) occurred at 233 °C. To examine the effect of $SrTiO_3$ addition on the activation energy (E_a) for hydrogen desorbed from $LiAlH_4$, different heating rates were measured using DSC. Fig. 4 shows the DSC curves for the 1-h milled $LiAlH_4$ and 10 wt% $SrTiO_3$-doped $LiAlH_4$ samples at several heating rates (15, 20, 25 and 30 °C/min).

The E_a values of the dehydrogenation process of the 1-h milled $LiAlH_4$ and $LiAlH_4$–10 wt% $SrTiO_3$ samples were obtained by applying the Kissinger equation [47] as follows:

$$\ln[\beta/T_p^2] = -E_a/RT_p + A \quad (1)$$

Thus, the E_a can be calculated from the slope in a plot of $\ln[\beta/T_p^2]$ versus $1000/T_p$ as shown in Fig. 5. As shown in the Kissinger plot, the E_a of the as-milled $LiAlH_4$ was 91 and 110 kJ/mol in the first and second dehydrogenation steps, respectively. After the addition of 10 wt% of $SrTiO_3$, the E_a of $LiAlH_4$ decreased notably. The E_a of the $LiAlH_4$–10 wt% $SrTiO_3$ sample was calculated to be 70 kJ/mol in the first step and 94 kJ/mol in the second step of dehydrogenation. Owing to the reduction of the E_a, the dehydrogenation properties of 10 wt% of $SrTiO_3$-doped $LiAlH_4$ were enhanced. Table 3 shows the apparent activation energy (E_a) of $LiAlH_4$ doped with different catalysts calculated by the Kissinger method.

Fig. 6 shows the powder morphology viewed by SEM for the commercial $LiAlH_4$, commercial $SrTiO_3$, 1-h milled $LiAlH_4$ and $LiAlH_4$–10 wt% $SrTiO_3$ samples. For the commercial $LiAlH_4$ sample (Fig. 6(a)), the image shows 'block-shaped' particles. The particle sizes were estimated to be between 10 and 50 μm. Meanwhile, the commercial $SrTiO_3$ particles have a spherical morphology with an inconsistent size (their average size was about 50 μm) as shown in Fig. 6(b). The images of $LiAlH_4$ after undergoing 60 min of ball milling showed agglomeration and an inhomogeneous distribution (their average size was 1–5 μm) as can be seen in Fig. 6(c). Compared to commercial $LiAlH_4$, clearly, the size of the particles decreased after the milling process. After doping with $SrTiO_3$ (Fig. 6(d)), the particle size reduced dramatically and showed less agglomeration than undoped $LiAlH_4$. It is reasonable to believe that the reduction in particle size accounts for the improvement in the desorption properties of the $SrTiO_3$-doped $LiAlH_4$ sample. A previous study revealed that smaller particles and less agglomeration in the metal/complex hydride–catalyst system provided more grain boundaries and higher surface areas and benefited the diffusion path for hydrogen during the dehydrogenation process [27].

Fig. 7 illustrates the XRD patterns of the commercial $SrTiO_3$, commercial $LiAlH_4$, 1-h milled $LiAlH_4$ and $LiAlH_4$–10 wt% $SrTiO_3$ samples after 1 h of milling. The commercial $LiAlH_4$ sample showed that only $LiAlH_4$ phases were detected, as presented in Fig. 7(a). Besides, the results of the XRD spectra after the milling process of $LiAlH_4$, as shown in Fig. 7(b), revealed that only $LiAlH_4$ phases were detected, indicating the high stability of $LiAlH_4$ during the ball milling process. This phenomenon is in good agreement with our previous studies [50–52]. Fig. 7(c) shows the XRD results after the addition of $SrTiO_3$, in which the peaks corresponding to $LiAlH_4$ still exist. In addition, new peaks corresponding to Al could also be detected for the $SrTiO_3$-doped $LiAlH_4$ sample, demonstrating that

Table 2
Comparison of dehydrogenation kinetic of $LiAlH_4$ doped with different catalysts.

System	Dehydrogenation temperature (°C)	Dehydrogenation time (min)	Hydrogen release (wt.%)
$LiAlH_4 + CoFe_2O_4$ [27]	90.0	20.0	1.4
$LiAlH_4 + ScCl_3$ [15]	150.0	20.0	1.8
$LiAlH_4 + NbN$ [42]	130.0	25.0	1.2
$LiAlH_4 + NiFe_2O_4$ [28]	90.0	25.0	1.5
$LiAlH_4 + FeCl_2$ [44]	110.0	50.0	2.0
$LiAlH_4 + MnFe_2O_4$ [45]	90.0	20.0	1.0
$LiAlH_4 + K_2TiF_6$ [46]	90.0	20.0	2.6
$LiAlH_4 + SrTiO_3$ [this work]	90.0	20.0	3.0

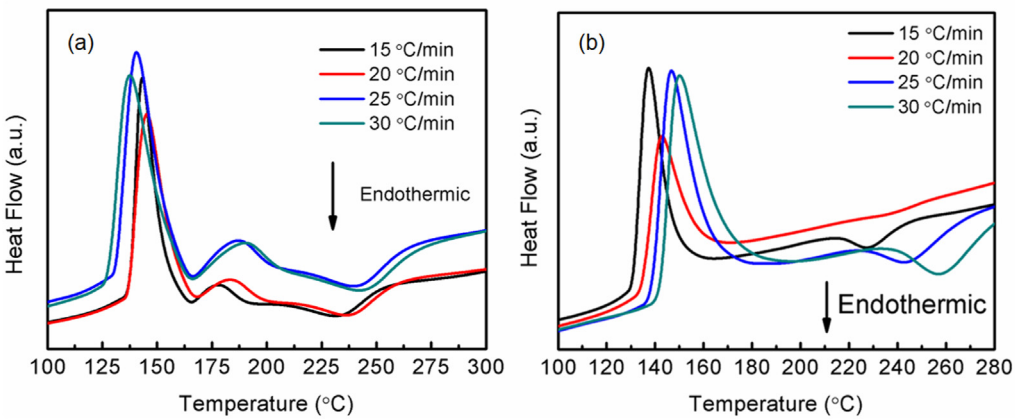

Fig. 4. Differential scanning calorimetry profiles of (a) 1 h milled $LiAlH_4$ and (b) $LiAlH_4$-10 wt% $SrTiO_3$ sample at different heating rates (15, 20, 25, and 30 °C/min).

$LiAlH_4$ decomposed slightly (Eq. (1)) during the mechanical milling process. Based on Eq. (1), the peaks of Li_3AlH_6 should have formed, but surprisingly no peak corresponding to Li_3AlH_4 was detected in the doped sample (Fig. 7(c)). This phenomenon is comparable to other studies in which TiF_3 and NbF_5-doped $LiAlH_4$ samples started decomposing during the milling process and no peak for Li_3AlH_6 could be detected from the XRD spectra [53,54]. In addition, $SrTiO_3$ peaks were detected, indicating that the additive does not react with the host material ($LiAlH_4$), similar to previous reports where $SrTiO_3$ phases were still stable after the mechanical milling and de/rehydrogenation processes [37–39]. The XRD results of commercial $SrTiO_3$ as shown in Fig. 7(d) indicate that the $SrTiO_3$ purchased was pure, as no other peak was detected except $SrTiO_3$ peaks.

FTIR analyses were carried out to confirm the existence of Li_3AlH_6 after the milling process of the $SrTiO_3$-doped $LiAlH_4$ sample as displayed in Fig. 8. From the results, an extra absorbance peak is obvious at around 1400 cm^{-1} for the $LiAlH_4$–10 wt% $SrTiO_3$ sample (Fig. 8(c)). This IR absorption peak can indicate the presence of Li_3AlH_6 (Al–H stretching mode) [29]. For the commercial and 1-h milled $LiAlH_4$ samples, as displayed in Fig. 8(a) and (b), only IR absorption peaks correlating to $LiAlH_4$ appeared; Li–Al–H bending modes occurred at 800–900 cm^{-1} and the Al–H stretching mode at 1600–1800 cm^{-1} [46], and no IR absorption peak was observed at about 1400 cm^{-1}. The FTIR results confirm that slight decomposition of $LiAlH_4$ (Eq. (1)) occurred during the milling process, in accordance with the XRD results (Fig. 7(c)).

Fig. 9 shows the XRD pattern of the 10 wt% $SrTiO_3$-doped $LiAlH_4$ sample after the complete dehydrogenation process at 250 °C (second step of dehydrogenation). As can be seen, the XRD pattern shows the LiH, Al and $SrTiO_3$ peaks; no peaks of $LiAlH_4$ and Li_3AlH_6 were detected. The presence of the LiH and Al peaks shows that the second step of the dehydrogenation process of $LiAlH_4$ has been completed (Eq. (1) and 2). The presence of the $SrTiO_3$ peaks proved that $SrTiO_3$ is hard to decompose and has not reacted with $LiAlH_4$ during the dehydrogenation process. In previous studies, we have shown that $SrTiO_3$ did not react with MgH_2 and Na_3AlH_6 during the ball milling and de/rehydrogenation processes [37–39].

Previous studies have revealed that the main catalytic role played by the additives or dopant in the $LiAlH_4$–catalyst system was as an *in-situ* active species formed during the milling or dehydrogenation process. The active species are believed to

Table 3
Comparison of apparent activation energy (E_a) of $LiAlH_4$ doped with different catalysts.

System	Activation energy (E_a) (kJ/mol)	
	First stage	Second stage
$LiAlH_4$ + K_2TiF_6 [46]	78.20	90.80
$LiAlH_4$ + Ti_3C_2 [48]	79.81	99.68
$LiAlH_4$ + $FeCl_2$ [44]	81.48	105.01
LiAlH4 + $ScCl_3$ [15]	82.30	93.20
$LiAlH_4$ + Co@C [49]	95.36	115.60
$LiAlH_4$ + $SrTiO_3$ [this work]	70.00	94.00

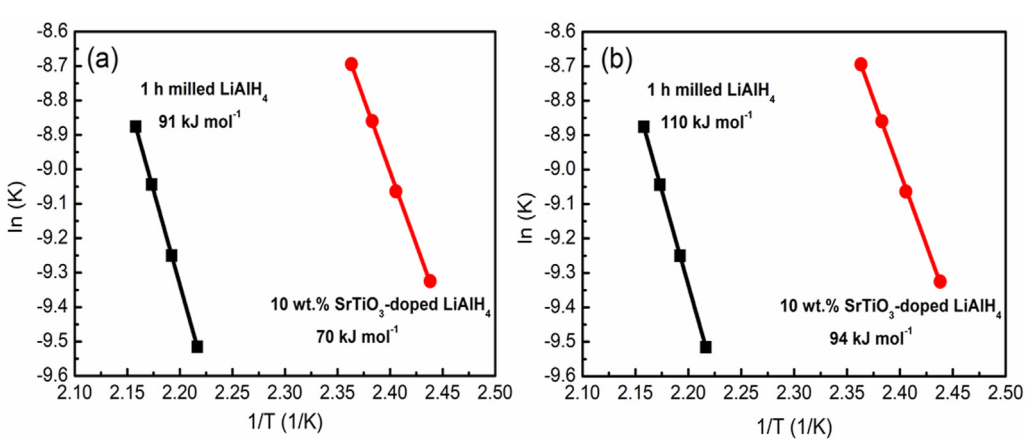

Fig. 5. Kissinger plots of (a) the first step dehydrogenation and (b) the second step dehydrogenation for 1 h milled $LiAlH_4$ and $LiAlH_4$-10 wt% $SrTiO_3$ sample.

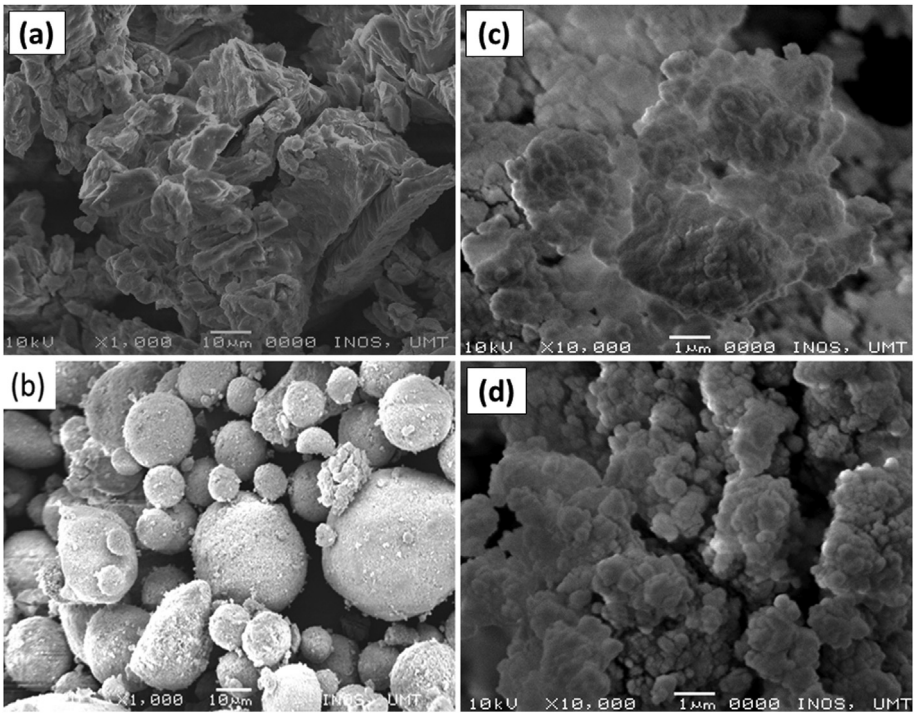

Fig. 6. SEM micrographs for (a) commercial $LiAlH_4$, (b) commercial $SrTiO_3$, (c) 1 h milled $LiAlH_4$, and (d) $LiAlH_4$-10 wt% $SrTiO_3$ sample.

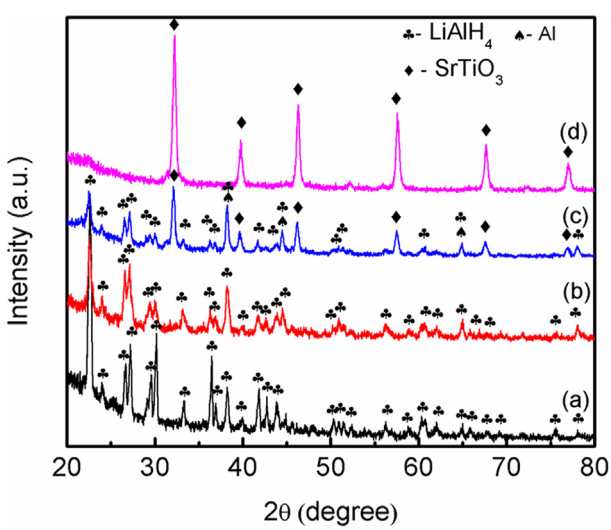

Fig. 7. XRD pattern for (a) commercial $LiAlH_4$, (b) 1 h milled $LiAlH_4$, (c) $LiAlH_4$-10 wt% $SrTiO_3$ after 1 h ball-mill and (d) commercial $SrTiO_3$.

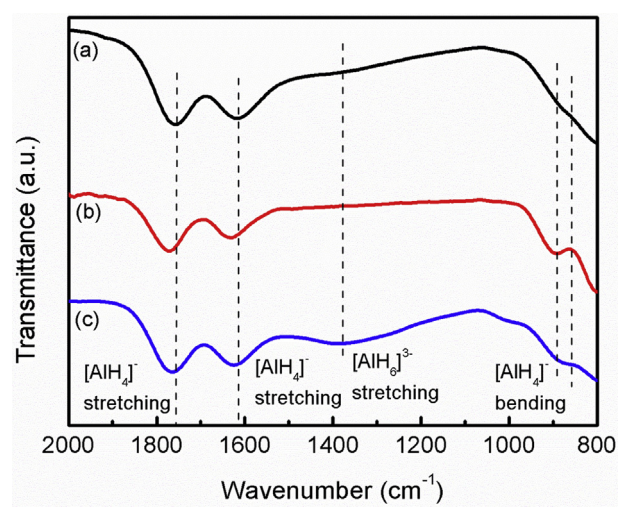

Fig. 8. FTIR pattern for (a) commercial $LiAlH_4$, (b) 1 h milled $LiAlH_4$ and (c) $LiAlH_4$-10 wt% $SrTiO_3$ after 60 min ball-mill.

improve the dehydrogenation properties by acting as the active sites for the nucleation and creation of the dehydrogenation yield by reducing the diffusion length of the reaction ions [45,55]. In the current study, the XRD results show that $SrTiO_3$ does not decompose or react with $LiAlH_4$ during the ball milling and dehydrogenation processes. Therefore, we hypothesised that $SrTiO_3$ plays a catalytic role owing to its hardness. $SrTiO_3$ is reported to have a hardness of 6.0–6.5 Mohs [56] compared with 4.0 Mohs of $LiAlH_4$. Therefore, adding $SrTiO_3$ into $LiAlH_4$ minimised the agglomeration of particles, and thus, this facilitated the refinement of $LiAlH_4$ particles during the milling process. It was reported previously that smaller particles in metal/complex hydrides improve the sorption properties [57]. In this study, smaller particles and less agglomeration in the $SrTiO_3$-doped $LiAlH_4$ sample (Fig. 6(d)) provided higher surface areas (increased grain boundaries) and benefited the diffusion path for hydrogen during the dehydrogenation process [36]. The hardness of the catalyst confers positive effects by improving the dehydrogenation characteristics of $LiAlH_4$ when $SrTiO_3$ is added. However, further characterisation such as that using transmission electron microscopy, is needed to elucidate in more detail the precise role of $SrTiO_3$ in enhancing the dehydrogenation properties of the $SrTiO_3$-doped $LiAlH_4$ catalyst system.

4. Conclusion

In conclusion, we have demonstrated that $SrTiO_3$ is an excellent

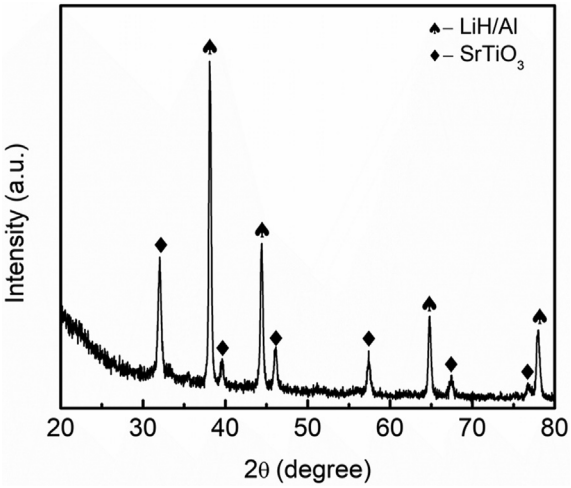

Fig. 9. X-ray diffraction pattern of $LiAlH_4$-10 wt% $SrTiO_3$ sample after dehydrogenation at 250 °C.

material to catalyse the desorption behaviours of $LiAlH_4$. The $LiAlH_4$–10 wt% $SrTiO_3$ sample starts to desorb H_2 at about 80 °C and 120 °C in the first and second dehydrogenation steps, respectively, reductions of about 65 °C and 58 °C compared to the milled $LiAlH_4$. For the desorption kinetic process at a fixed temperature of 90 °C, the $LiAlH_4$–10 wt% $SrTiO_3$ sample can release about 4.0 wt% of H_2 in 60 min compared to 0.3 wt% released by the pure ball milled $LiAlH_4$. Kissinger analysis showed that the E_a in the first and second dehydrogenation steps for pure ball milled $LiAlH_4$ decreased from 91 and 110 kJ/mol to 70 and 94 kJ/mol, respectively, by the addition of 10 wt% $SrTiO_3$. In the XRD spectra post ball milling for the doped sample, there are peaks matching Al, indicating that the addition of $SrTiO_3$ encourages the slight decomposition of $LiAlH_4$ during the milling process. The XRD pattern also showed that $SrTiO_3$ did not decompose or react with the host material during the milling and dehydrogenation processes. $SrTiO_3$ is assumed to play a catalytic role by reducing the particle size of $LiAlH_4$ during the milling process. Small particles of $LiAlH_4$ will increase the grain boundaries and surface areas and consequently improve the dehydrogenation properties of $LiAlH_4$.

CRediT authorship contribution statement

M. Ismail: Supervision, Writing - original draft, Methodology, Formal analysis. **N.A. Sazelee:** Formal analysis, Writing - review & editing. **N.A. Ali:** Formal analysis, Writing - review & editing. **S. Suwarno:** Writing - review & editing.

Declaration of competing interest

The authors declare that they have no known competing financial interests or personal relationships that could have appeared to influence the work reported in this paper.

Acknowledgements

Financial support from the Universiti Malaysia Terengganu through the Golden Goose Research Grant (VOT 55190) is greatly acknowledged.

References

[1] I.P. Jain, Hydrogen the fuel for 21st century, Int. J. Hydrogen Energy 34 (2009) 7368–7378.
[2] I.P. Jain, P. Jain, A. Jain, Novel hydrogen storage materials: a review of light-weight complex hydrides, J. Alloys Compd. 503 (2011) 303–339.
[3] L. Ouyang, K. Chen, J. Jiang, X.-S. Yang, M. Zhu, Hydrogen storage in light-metal based systems: a review, J. Alloys Compd. 829 (2020) 154597.
[4] L. Ouyang, F. Liu, H. Wang, J. Liu, X.-S. Yang, et al., Magnesium-based hydrogen storage compounds: a review, J. Alloys Compd. 832 (2020) 154865.
[5] N.A. Ali, N.H. Idris, M.F.M. Din, N.S. Mustafa, N.A. Sazelee, et al., Nanolayer-like-shaped $MgFe_2O_4$ synthesised via a simple hydrothermal method and its catalytic effect on the hydrogen storage properties of MgH_2, RSC Adv. 8 (2018) 15667–15674.
[6] N.H. Idris, N.S. Mustafa, M. Ismail, $MnFe_2O_4$ nanopowder synthesised via a simple hydrothermal method for promoting hydrogen sorption from MgH_2, Int. J. Hydrogen Energy 42 (2017) 21114–21120.
[7] N.H. Idris, A.S.K. Anuar, N.A. Ali, M. Ismail, Effect of K_2NbF_7 on the hydrogen release behaviour of $NaAlH_4$, J. Alloys Compd. 851 (2021) 156686.
[8] U.S. Department of Energy (Doe), Hydrogen storage targets for onboard light-duty vehicle. https://www.energy.gov/sites/prod/files/2017/05/f34/fcto_targets_onboard_hydro_storage_explanation.pdf, 2020.
[9] A. Andreasen, T. Vegge, A.S. Pedersen, Dehydrogenation kinetics of as-received and ball-milled $LiAlH_4$, J. Solid State Chem. 178 (2005) 3672–3678.
[10] R.A. Varin, L. Zbroniec, Decomposition behavior of unmilled and ball milled lithium alanate ($LiAlH_4$) including long-term storage and moisture effects, J. Alloys Compd. 504 (2010) 89–101.
[11] Y. Zhang, Q.-F. Tian, S.-S. Liu, L.-X. Sun, The destabilization mechanism and de/re-hydrogenation kinetics of MgH_2-$LiAlH_4$ hydrogen storage system, J. Power Sources 185 (2008) 1514–1518.
[12] Y. Yang, M. Gao, Y. Liu, J. Wang, J. Gu, et al., Multi-hydride systems with enhanced hydrogen storage properties derived from $Mg(BH_4)_2$ and $LiAlH_4$, Int. J. Hydrogen Energy 37 (2012) 10733–10742.
[13] N.S. Mustafa, M. Ismail, Enhanced hydrogen storage properties of $4MgH_2$ + $LiAlH_4$ composite system by doping with Fe_2O_3 nanopowder, Int. J. Hydrogen Energy 39 (2014) 7834–7841.
[14] N.A. Ali, N.H. Idris, N.A. Sazelee, M.S. Yahya, F.A.H. Yap, et al., Catalytic effects of $MgFe_2O_4$ addition on the dehydrogenation properties of $LiAlH_4$, Int. J. Hydrogen Energy 44 (2019) 28227–28234.
[15] Z. Cao, X. Ma, H. Wang, L. Ouyang, Catalytic effect of $ScCl_3$ on the dehydrogenation properties of $LiAlH_4$, J. Alloys Compd. 762 (2018) 73–79.
[16] N.A. Sazelee, M.S. Yahya, N.H. Idris, M.F. Md Din, M. Ismail, Desorption properties of $LiAlH_4$ doped with $LaFeO_3$ catalyst, Int. J. Hydrogen Energy 44 (2019) 11953–11960.
[17] Y. Zhu, L. Ouyang, H. Zhong, J. Liu, H. Wang, et al., Closing the loop for hydrogen storage: facile regeneration of $NaBH_4$ from its hydrolytic product, Angew. Chem. Int. Ed. 59 (2020) 8623–8629.
[18] K. Chen, L. Ouyang, H. Zhong, J. Liu, H. Wang, et al., Converting H^+ from co-ordinated water into H^- enables super facile synthesis of $LiBH_4$, Green Chem. 21 (2019) 4380–4387.
[19] L. Ouyang, W. Chen, J. Liu, M. Felderhoff, H. Wang, et al., Enhancing the regeneration process of consumed $NaBH_4$ for hydrogen storage, Adv. Energy Mater. 7 (2017) 1700299.
[20] Z.H. Tan, L.Z. Ouyang, J.M. Huang, J.W. Liu, H. Wang, et al., Hydrogen generation via hydrolysis of Mg_2Si, J. Alloys Compd. 770 (2019) 108–115.
[21] Z. Tan, L. Ouyang, J. Liu, H. Wang, H. Shao, et al., Hydrogen generation by hydrolysis of Mg-Mg_2Si composite and enhanced kinetics performance from introducing of $MgCl_2$ and Si, Int. J. Hydrogen Energy 43 (2018) 2903–2912.
[22] X. Yu, Z. Tang, D. Sun, L. Ouyang, M. Zhu, Recent advances and remaining challenges of nanostructured materials for hydrogen storage applications, Prog. Mater. Sci. 88 (2017) 1–48.
[23] R.A. Varin, R. Parviz, The effects of the micrometric and nanometric iron (Fe) additives on the mechanical and thermal dehydrogenation of lithium alanate ($LiAlH_4$), its self-discharge at low temperatures and rehydrogenation, Int. J. Hydrogen Energy 37 (2012) 9088–9102.
[24] R.A. Varin, L. Zbroniec, The effects of nanometric nickel (n-Ni) catalyst on the dehydrogenation and rehydrogenation behavior of ball milled lithium alanate ($LiAlH_4$), J. Alloys Compd. 506 (2010) 928–939.
[25] Z. Xueping, L. Ping, A. Fuqiang, W. Guoqing, Q. Xuanhui, Effects of Ti and Fe additives on hydrogen release from lithium alanate, Rare Met. Mater. Eng. 37 (2008) 400–403.
[26] Z. Li, P. Li, Q. Wan, F. Zhai, Z. Liu, et al., Dehydrogenation improvement of $LiAlH_4$ catalyzed by Fe_2O_3 and Co_2O_3 nanoparticles, J. Phys. Chem. C 117 (2013) 18343–18352.
[27] Z. Li, F. Zhai, Q. Wan, Z. Liu, J. Shan, et al., Enhanced hydrogen storage properties of $LiAlH_4$ catalyzed by $CoFe_2O_4$ nanoparticles, RSC Adv. 4 (2014) 18989–18997.
[28] P. Li, Z. Li, F. Zhai, Q. Wan, X. Li, et al., $NiFe_2O_4$ nanoparticles catalytic effects of improving $LiAlH_4$ dehydrogenation properties, J. Phys. Chem. C 117 (2013) 25917–25925.
[29] J.R. Ares Fernandez, F. Aguey-Zinsou, M. Elsaesser, X.Z. Ma, M. Dornheim, et al., Mechanical and thermal decomposition of $LiAlH_4$ with metal halides, Int. J. Hydrogen Energy 32 (2007) 1033–1040.
[30] L. Shenglin, M. Qiuhua, L. Heng, Z. Xueping, F. Xin, et al., Effect of F^{-1} on the hydrogen release properties of $NaAlH_4$ and $LiAlH_4$, Rare Met. Mater. Eng. 43 (2014) 61–63.
[31] C.-P. Hsu, D.-h. Jiang, S.-L. Lee, J.-L. Horng, M.-D. Ger, et al., Buckyball-, carbon nanotube-, graphite-, and graphene-enhanced dehydrogenation of lithium

aluminum hydride, Chem. Commun. 49 (2013) 8845–8847.
[32] W.-C. Hsu, C.-H. Yang, W.-T. Tsai, Catalytic effect of MWCNTs on the dehydrogenation behavior of $LiAlH_4$, Int. J. Hydrogen Energy 39 (2014) 927–933.
[33] Rafi-ud-din, L. Zhang, L. Ping, Q. Xuanhui, Catalytic effects of nano-sized TiC additions on the hydrogen storage properties of $LiAlH_4$, J. Alloys Compd. 508 (2010) 119–128.
[34] Rafi-ud-din, X. Qu, P. Li, M. Ahmad, Z. Lin, Comparative catalytic effects of $NiCl_2$, TiC and TiN on hydrogen storage properties of $LiAlH_4$, Rare Met. 30 (2011) 27–34.
[35] M.-Q. Fan, S.-S. Liu, Y. Zhang, J. Zhang, L.-X. Sun, et al., Superior hydrogen storage properties of MgH_2-10 wt.% TiC composite, Energy 35 (2010) 3417–3421.
[36] A. Ranjbar, Z.P. Guo, X.B. Yu, D. Wexler, A. Calka, et al., Hydrogen storage properties of MgH_2-SiC composites, Mater. Chem. Phys. 114 (2009) 168–172.
[37] M.S. Yahya, M. Ismail, Catalytic effect of $SrTiO_3$ on the hydrogen storage behaviour of MgH_2, J. Energy Chem. 28 (2019) 46–53.
[38] M.S. Yahya, W.B. Lew, F.A. Halim Yap, M. Ismail, The catalytic effect of an inert additive ($SrTiO_3$) on the hydrogen storage properties of $4MgH_2$-Na_3AlH_6, Int. J. Hydrogen Energy 43 (2018) 20801–20810.
[39] M.S. Yahya, M. Ismail, Synergistic catalytic effect of $SrTiO_3$ and Ni on the hydrogen storage properties of MgH_2, Int. J. Hydrogen Energy 43 (2018) 6244–6255.
[40] S.-S. Liu, Z.-B. Li, C.-L. Jiao, X.-L. Si, L.-N. Yang, et al., Improved reversible hydrogen storage of $LiAlH_4$ by nano-sized TiH_2, Int. J. Hydrogen Energy 38 (2013) 2770–2777.
[41] L. Li, F. Qiu, Y. Wang, Y. Xu, C. An, et al., Enhanced hydrogen storage properties of TiN–$LiAlH_4$ composite, Int. J. Hydrogen Energy 38 (2013) 3695–3701.
[42] L. Li, Y. Xu, Y. Wang, Y. Wang, F. Qiu, et al., NbN nanoparticles as additive for the high dehydrogenation properties of $LiAlH_4$, Dalton Trans. 43 (2013) 1806–1813.
[43] Rafi-ud-din, Q. Xuanhui, L. Ping, L. Zhang, M. Ahmad, Hydrogen sorption improvement of $LiAlH_4$ catalyzed by Nb_2O_5 and Cr_2O_3 nanoparticles, J. Phys. Chem. C 115 (2011) 13088–13099.
[44] J. Cai, L. Zang, L. Zhao, J. Liu, Y. Wang, Dehydrogenation characteristics of $LiAlH_4$ improved by in-situ formed catalysts, J. Energy Chem. 25 (2016) 868–873.
[45] F. Zhai, P. Li, A. Sun, S. Wu, Q. Wan, et al., Significantly improved dehydrogenation of $LiAlH_4$ destabilized by $MnFe_2O_4$ nanoparticles, J. Phys. Chem. C 116 (2012) 11939–11945.
[46] Z. Li, S. Liu, X. Si, J. Zhang, C. Jiao, et al., Significantly improved dehydrogenation of $LiAlH_4$ destabilized by K_2TiF_6, Int. J. Hydrogen Energy 37 (2012) 3261–3267.
[47] H.E. Kissinger, Reaction kinetics in differential thermal analysis, Anal. Chem. 29 (1957) 1702–1706.
[48] Y. Xia, H. Zhang, Y. Sun, L. Sun, F. Xu, et al., Dehybridization effect in improved dehydrogenation of $LiAlH_4$ by doping with two-dimensional Ti_3C_2, Mater, Today Nano 8 (2019) 100054.
[49] L. Li, Y. Wang, L. Jiao, H. Yuan, Enhanced catalytic effects of Co@C additive on dehydrogenation properties of $LiAlH_4$, J. Alloys Compd. 645 (2015) S468–S471. Supplement 1.
[50] N.A. Ali, N. Sazelee, M.S. Yahya, M. Ismail, Influence of K_2NbF_7 catalyst on the desorption behavior of $LiAlH_4$, Front. Chem. 8 (2020) 457.
[51] N.A. Sazelee, M.S. Yahya, N.A. Ali, N.H. Idris, M. Ismail, Enhancement of dehydrogenation properties in $LiAlH_4$ catalysed by $BaFe_{12}O_{19}$, J. Alloys Compd. 835 (2020) 155183.
[52] N.N. Sulaiman, M. Ismail, Catalytic effect of $SrFe_{12}O_{19}$ on the hydrogen storage properties of $LiAlH_4$, Int. J. Hydrogen Energy 42 (2017) 19126–19134.
[53] S.-S. Liu, L.-X. Sun, Y. Zhang, F. Xu, J. Zhang, et al., Effect of ball milling time on the hydrogen storage properties of TiF_3-doped $LiAlH_4$, Int. J. Hydrogen Energy 34 (2009) 8079–8085.
[54] M. Ismail, Y. Zhao, X.B. Yu, S.X. Dou, Effects of NbF_5 addition on the hydrogen storage properties of $LiAlH_4$, Int. J. Hydrogen Energy 35 (2010) 2361–2367.
[55] P. Li, Q. Wan, Z. Li, F. Zhai, Y. Li, et al., MgH_2 dehydrogenation properties improved by $MnFe_2O_4$ nanoparticles, J. Power Sources 239 (2013) 201–206.
[56] J.W. Anthony, R.A. Bideaux, K.W. Bladh, M.C. Nichols, Handbook of Mineralogy, Mineral Data Publ, Tucson, 1990.
[57] A. Ranjbar, M. Ismail, Z.P. Guo, X.B. Yu, H.K. Liu, Effects of CNTs on the hydrogen storage properties of MgH_2 and MgH_2-BCC composite, Int. J. Hydrogen Energy 35 (2010) 7821–7826.